Separation of the σ_L and σ_T contributions to the production of hadrons in hard lepto-scattering

H. Avakian and N. Sato

Thomas Jefferson National Accelerator Facility, Newport News, Virginia 23606

R. Capobianco

University of Connecticut, Storrs, Connecticut 06269 and Argonne National Laboratory, Lemont, Illinois 60439

T.B. Hayward, K. Joo, A. Kim, and U. Shrestha

University of Connecticut, Storrs, Connecticut 06269

S. Diehl

II. Physikalisches Institut der Universität Gießen, 35392 Gießen, Germany and University of Connecticut, Storrs, Connecticut 06269

M. Scott and M. Zurek

Argonne National Laboratory, Lemont, Illinois 60439

The separation and evaluation of the contribution of longitudinal photons is of critical importance to the understanding of the systematics in phenomenology used to extract the underlying 3D parton distributions from measurements of multiplicities and azimuthal asymmetries in the semi-inclusive and hard exclusive production of hadrons. We propose an addition to the Run Group K experiments in Hall B, focusing on performing an in-depth analysis of the cross sections for the production of hadrons in lepto-scattering. By comparing the obtained results with those from Run Group A, conducted at a higher beam energy, and performing a Rosenbluth separation we aim to disentangle the contributions from transversely and longitudinally polarized photons. The Rosenbluth separation is performed empirically by measuring the semi-inclusive leptoproduction cross section at a set of kinematics corresponding to the same photon 4-momentum Q^2 and longitudinal momentum x, but at different ratios of longitudinal to transverse photon polarization ϵ. This requires measurements at different combinations of incident electron energy and scattering

angle. While moderately accurate measurements of the ratio R_{DIS} of longitudinal to transverse cross section exist for inclusive deep inelastic scattering, there have been no measurements of R_{SIDIS} for the SIDIS process. Our study aims to fill this gap in knowledge and provide valuable insights into the nucleon structure and quark-gluon dynamics. To facilitate this study, we request beam time with an inbending torus polarity, enabling the measurement of higher values of Q^2.

CONTENTS

I. Introduction 4
A. Semi-inclusive Deep Inelastic Scattering 4
B. σ_L/σ_T separation 5
C. Previous R_{SIDIS} Measurements 6
D. Preliminary CLAS12 Measurements 7
1. RGA Analysis of $\cos\phi$ and $\cos 2\phi$ Modulations 7
2. Example extraction of R_{SIDIS} 7
E. The Need for Inbending 9

II. Experimental Set up 10

III. Monte Carlo 11
A. Description 11
B. MC Event Matching 11
C. Monte Carlo Smearing 12
D. Data vs MC Comparison 12

IV. Analysis Procedure 16
A. Particle Identification and Fiducial Cuts 16
B. Channel Selection 16
C. Rosenbluth Separation 17
D. Minor Systematic Uncertainties 22
E. Acceptance Correction 22
F. Radiative Effects 22
G. Total systematic uncertainty 23

V. Conclusions 24

References 24

I. INTRODUCTION

A. Semi-inclusive Deep Inelastic Scattering

Semi-inclusive deep inelastic scattering (SIDIS), where an electron scatters off a nucleon target at a high enough energy such that it can be described by the scattering off a single parton in the target [1], is a powerful tool for investigating the nucleon structure and quark-gluon dynamics. If the final state hadrons are produced from the struck quark the cross section can be factorized into a two stage process [2]. The first stage is described by PDFs [3, 4], which describe the probability of finding a specific quark or gluon in a particular state inside the nucleon. The second stage is dictated by fragmentation functions (FFs) [5], which govern the formation of hadrons out of quarks and gluons. A consequence of this factorization is that the first stage depends on x and not on z and vice-versa for the second stage, but both depend on Q^2 (variables defined below).

In SIDIS experiments, cross sections for various hadron production processes provide essential information about the underlying quark distributions and their interactions within the nucleon. The SIDIS cross section can be expressed in terms of longitudinal and transverse contributions from virtual photons along with their interference terms [2, 6, 7]:

$$\frac{d\sigma}{dxdQ^2dzdP_T^2d\phi} = \frac{\pi\alpha^2}{x^2Q^4}\frac{(2x+\gamma^2)}{(1+\gamma^2)}K(y)\left(F_{UU,T} + \epsilon F_{UU,L} + \sqrt{2\epsilon(1+\epsilon)}\cos\phi F_{UU}^{\cos\phi} + \epsilon\cos(2\phi)F_{UU}^{\cos(2\phi)}\right). \tag{1}$$

The structure functions (SFs), represented by $F_{UU,T}$, $F_{UU,L}$, $F_{UU}^{\cos\phi}$, and $F_{UU}^{\cos(2\phi)}$, play a crucial role in describing the nucleon's internal structure as they encode information about the quark distributions and their interactions within the nucleon. The subscripts in the structure functions $F_{UU,LU,\ldots}$, specify the beam (first index) and target (second index) polarization, U, L for the unpolarized and longitudinally polarized case, respectively. The depolarization factors represent the fraction of the initial electron polarization that is transferred to the virtual photon, which influences the virtual photon's polarization state and are described by the variable

$$K(y) = 1 - y + y^2/2 + \gamma^2y^2/4, \qquad \varepsilon = \frac{1 - y - \frac{1}{4}\gamma^2y^2}{1 - y + \frac{1}{2}y^2 + \frac{1}{4}\gamma^2y^2}, \tag{2}$$

with γ, x, y and Q^2 defined below. Additional variables, relevant for all SIDIS analyses, are given by

$$Q^2 = -q^2, \tag{3}$$

$$W^2 = (P+q)^2, \tag{4}$$

$$\nu = \frac{q \cdot P}{M} = E - E', \tag{5}$$

$$x = \frac{Q^2}{2P \cdot q} = \frac{Q^2}{2M\nu}, \tag{6}$$

$$y = \frac{P \cdot q}{P \cdot \ell} = \frac{\nu}{E}, \tag{7}$$

$$z = \frac{P \cdot P_h}{P \cdot q} = \frac{E_h}{\nu}, \tag{8}$$

$$\gamma = \frac{2Mx}{Q} = \frac{Q}{\nu}, \tag{9}$$

$$P_T = P_h \sin\theta_{\gamma h}, \tag{10}$$

The four-momentum of the exchanged virtual photon is defined as $q = l - l'$ such that $Q^2 = -q^2$ is the hard scale of the process (the virtuality of the exchanged photon). Conversely, W is the mass of the virtual photon, target system (the "hadronic mass"). If the electron beam has energy E and the scattered electron has energy E' then ν is defined as the difference between these two quantities. The variables x, y, and z are, respectively, the fraction of target momentum carried by the struck quark, the fraction of beam energy transferred to the virtual photon, and the fraction of virtual photon energy carried by the hadron system. The quantity γ describes the relationship between the energy transferred to the struck quark and the energy of the virtual photon. If $\theta_{\gamma h}$ is the angle between the hadron momentum and the virtual photon momentum, then P_T is the projection of P_h perpendicular to the virtual photon direction.

B. σ_L/σ_T separation

It is necessary to separate experimentally the relevant SFs that contribute to different multiplicities and azimuthal modulations, in a given multidimensional space with controlled systematics, to get a realistic physics interpretation of experimental observables. Some of the most prominent SFs include the unpolarized SF, $F_{UU,T}$ and the Sivers function, $F_{UU,T}^{\sin(\phi-\phi_s)}$, which are related to contributions from transversely polarized photons. Despite receiving less study, the contributions from longitudinally polarized photons, which contribute to the same observables, are expected to be significant in all accessible kinematics in polarized SIDIS. The evaluation of the separate contributions from longitudinally and transversely polarized photons requires measurements with different beam energies with a wide enough gap to provide some variation of the ratio, R, of the longitudinal to transverse cross sections. Theoretical investigations of the longitudinal SFs have so far been hindered by their twist-4 nature. The complete twist-4 result for semi-inclusive deep inelastic scattering with polarized electron and proton beams at the tree level in perturbative quantum chromodynamics (pQCD) [8], reveals significant contributions, in particular at large transverse momenta. The longitudinal photon contributions are expected to be more significant in the exclusive and semi-exclusive production for vector mesons in particular. Separation of the contributions from longitudinally polarized photons and measurements of the relative fraction R, Where $R = \sigma_L/\sigma_T$ will be critical for understanding systematics in all phenomenological extractions of polarized SIDIS measurements.

C. Previous R_{SIDIS} Measurements

While moderately accurate measurements of the ratio R_{DIS} exist for the ratio of longitudinal to transverse cross sections for inclusive deep inelastic scattering, there are essentially no measurements of R_{SIDIS} for the SIDIS process. Previous measurements of pion electroproduction at moderate Q^2 and W were performed at the Cornell synchrotron in the 1970s at values of ϵ separated by less than 0.1 and averaged over ϕ and $P_T < 0.2$ GeV. These data allowed for the extraction of R_{SIDIS}, albeit with a very large uncertainty [9].

More recent SIDIS measurements at HERMES, COMPASS, and Jefferson Lab have assumed $R_{\mathrm{SIDIS}} = R_{DIS}$, which is independent of z, p_T, and ϕ, as well as hadron and target nucleon identities. The assumption of $R_{\mathrm{SIDIS}} = R_{DIS}$ introduces significant uncertainties when using SIDIS data to infer quark flavor and spin distributions. Given the origin of contributions from longitudinal photons [8], with an expected strong dependence on the transverse momentum of hadrons, that assumption is very likely to introduce significant systematics, practically uncontrolled at large non-perturbative transverse momenta. Incidentally, this region is where most of the disagreements were observed in phenomenological attempts to describe the data from HERMES and COMPASS. To address this issue and improve our understanding of the nucleon structure, it is crucial to obtain direct measurements of R_{SIDIS}.

The structure function $F_{UU,L}$, which represents the longitudinal component of the SIDIS cross section, can be computed at order α_S, where α_S is the fine structure constant, and leading twist. In the transverse momentum dependent (TMD) case, $F_{UU,L}$ can also be computed at high transverse momentum and is predicted to be equal to twice the structure function $F_{UU}^{\cos 2\phi_h}$ [10]. Previous measurements have shown that this structure function is of the same order of magnitude as the $F_{UU,T}$ structure function. The R_{DIS} evaluated from measurements of F_L at HERA using 3 beam energies, for $Q^2 \geq 3.5$ GeV^2 shows a constant behaviour with $R = 0.260 \pm 0.050$ [11]. Similar results were obtained at JLab at lower beam energies [12]. In non-perturbative kinematics in SIDIS, particularly at relatively large transverse momenta, it is possible that this ratio can even exceed unity.

D. Preliminary CLAS12 Measurements

1. *RGA Analysis of* $\cos\phi$ *and* $\cos 2\phi$ *Modulations*

Semi-inclusive deep inelastic π^+ electroproduction has been studied with the CLAS12 detector at Jefferson Laboratory. The analyzed data was taken with a polarized 10.6 GeV electron beam, interacting with an unpolarized liquid hydrogen target and a negative (inbending) torus polarity. The collected statistics enable a high-precision study of the $\cos\phi$ and $\cos 2\phi$ azimuthal moments of the unpolarized cross-sections. These azimuthal moments may probe the Boer-Mulders function, which describes the net transverse polarization of quarks inside an unpolarized proton, and the Cahn effect, which has a purely kinematic origin. In Fig. 1 some preliminary extractions of the unfolded ϕ distribution are shown for several z-P_T bins in one particular Q^2-x_b bin. At high P_T (top of the plot) the relative contributions of the $\cos\phi$ amplitude are much larger than the $\cos 2\phi$, while at lower P_T the two amplitudes are similar in magnitude. The $\cos\phi$ amplitude, which corresponds to the so-called $d\sigma_{LT}/dt$ part of the cross section, receives significant contributions from longitudinal photons. Studying this P_T dependence, where the RGA data already implies a changing R_{SIDIS} value with P_T, will be a main goal of this proposal.

2. *Example extraction of* R_{SIDIS}

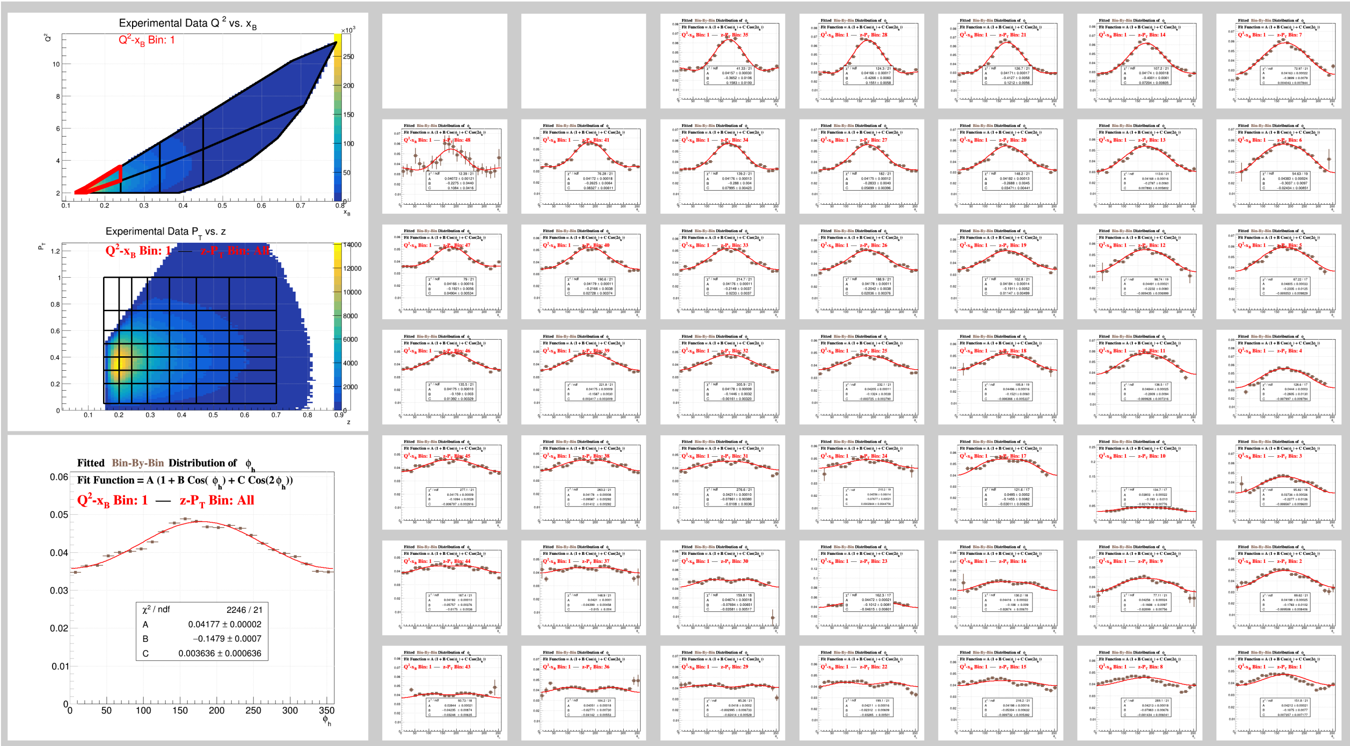

FIG. 1: **Preliminary** ϕ_h unfolded distributions for the $ep \to e'\pi^+X$ channel using the Bayesian Unfolding method. Plots show the distributions within Q^2-x_B Bin 1 (highlighted in red) and in each of the individual z-P_T bins (P_T increases from top to bottom and z increases from left to right). Each plot has been fitted with an equation of the form $A(1 + B\cos\phi + C\cos 2\phi)$, where $A = A_0(1 + \epsilon R_{\text{SIDIS}})$ for the purpose of this proposal.

E. The Need for Inbending

Another motivation for extending the measurement to the inbending torus polarity is the improved ϕ coverage of the π^+ for the negative torus field setting. In Fig. 2 the reconstructed ϕ distribution for π^+ and π^- are shown for the inbending and outbending torus polarities. For the $\pi^+(\pi^-)$ in outbending(inbending) there is a large gap from approximately $-60°$ to $+60°$ degrees. This gap could complicate any extractions and introduce additional systematics into the determination of R_{SIDIS}. The dramatic effect is also easily seen in a 2D plot of P_T vs. ϕ shown in Fig. 2 for the 7.5 GeV (chosen as an example; the effect is largely identical regardless of beam energy) energy setting.

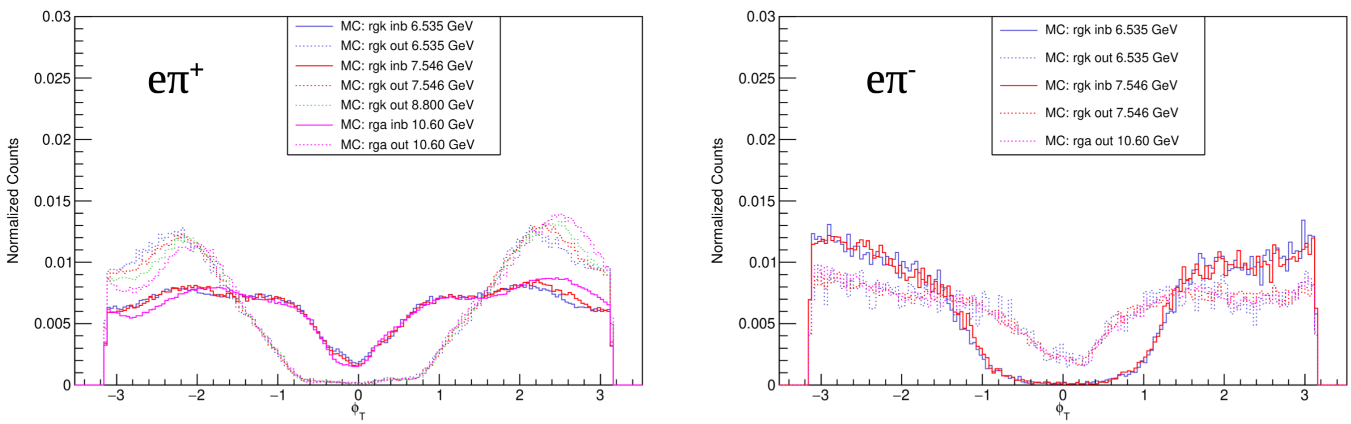

FIG. 2: Comparison between the reconstructed ϕ distributions for π^+ (left) and π^- (right) for the inbending and outbending torus polarities of CLAS12 at three different beam energies. A large gap in coverage can be seen for the outbending data around $\phi = 0$ for the π^+ case which is of principle interest.

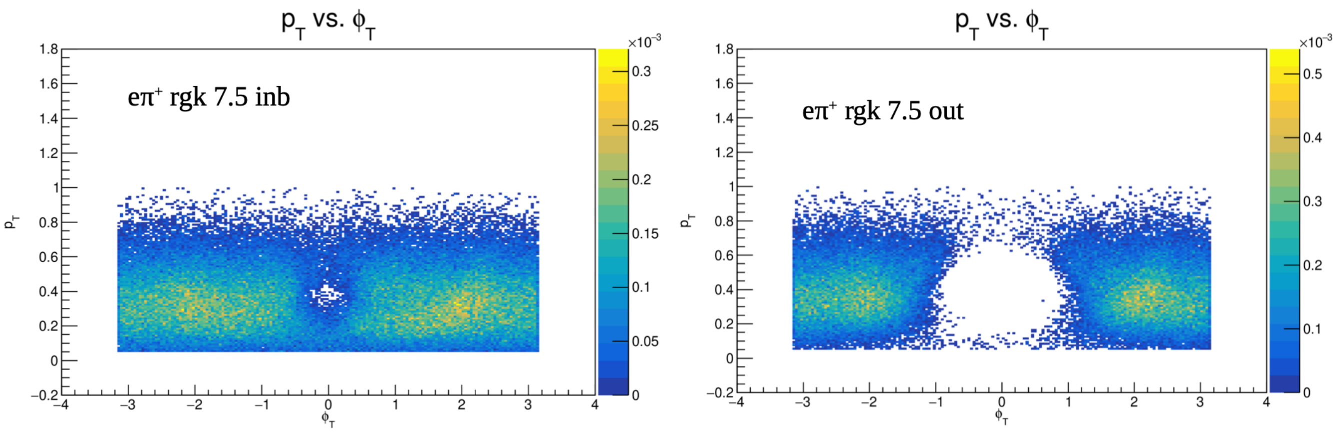

FIG. 3: P_T vs. ϕ coverage for the 7.5 GeV electron beam for inbending (left) and outbending (right). A significant hole exists in the outbending data that will complicate extractions.

II. EXPERIMENTAL SET UP

The proposed measurements will be conducted using the CLAS12 detector [13] in the previously approved RG-K configuration, following a similar approach to other approved SIDIS studies [14–19]. These studies involve longitudinally polarized proton and deuteron targets. The CLAS12 system is an upgrade of the original CLAS detector and features a new dual magnetic field system. This system includes a superconducting solenoid magnet for momentum reconstruction within the polar angle range of 5° to 45°, and a torus magnet that allows for nearly complete 360° azimuthal coverage.

The CLAS12 detector is divided into six independent sectors, each providing one-sixth of the total azimuthal coverage. Additionally, the detector is separated into the Forward Detector (FD) and Central Detector (CD) systems. The FD of CLAS12 is responsible for detecting particles scattered at angles below approximately 35°. It comprises Cherenkov counters [20, 21], a dedicated ring imaging Cherenkov counter for pion/kaon discrimination [22], drift chambers [23], time-of-flight scintillators [24], and electromagnetic calorimeters [25].

On the other hand, the CD detects particles deflected at larger angles, ranging from approximately 35° to 125°. It consists of a silicon vertex tracker [26], a central time of flight system [27], and a central vertex tracker [28]. The solenoid used for the central tracker also serves to generate the magnetic field required for the polarized target.

III. MONTE CARLO

A. Description

The CLAS12 Fall 2018 RG-A experimental configuration has been described in detail in GEMC [29], a GEANT4 based simulation package that offers the possibility to easily implement detectors in a full GEANT simulation. The position of the detectors in Hall B have been matched to survey data and a realistic map of the magnetic field has been generated to accurately reproduce the experimental set up. LUND generators were used to produce realistic final states that were read by GEMC version 4.3.2 and passed through the the detector system of CLAS12. The results of this process were cooked with COATJAVA version 6.5.3 will need updated for RGK simulations and the reconstructed banks were added to the original generated banks for comparison. The generator used for SIDIS Monte Carlo analysis is clasdis [30] which is based on the PEPSI generator [31, 32], the polarized version of the well-known LEPTO generator [33].

B. MC Event Matching

In order to evaluate the effects of several systematics, such as bin migration effects, it is necessary to be able to match particles created in the Event Generator and "detected" particles after they have been processed by the GEMC detector simulation and particle reconstruction of CLAS12. Unfortunately, at the time of this proposal no strict truth matching was included in the Monte Carlo process in order to be able to match tracks before and after reconstruction with full certainty. Instead, a requirement of matching electric charge (as measured by curvature in the magnetic field) and restrictions on the lab-frame angles of the tracks, $\Delta\phi < 6^\circ$ and $\Delta\theta < 2^\circ$, were used in order to pair generated and reconstructed particles. The effect of subtly altering this requirement by varying the strictness of the angular cuts was studied in the thesis of Timothy Hayward, pg. 85 [34], in the RGA Common Analysis note [35] and in other CLAS12 SIDIS analyses. No dramatic dependence was observed and the differences correspond to sub-permil levels which are much smaller than any uncertainties on the Monte Carlo models themselves. A requirement of matching particle identification is not enforced because this is one of the important systematics to study (e.g. the rate of kaons misidentified as pions).

C. Monte Carlo Smearing

It has been observed in previous CLAS12 analyses that the resolution of the Monte Carlo is superior to that of reconstructed data. In the preliminary $\cos\phi$ and $\cos 2\phi$ analysis of RGA data a particle-dependent smearing function has been developed for electrons and pions in order to better mimic realistic resolution effects. The modifications were made by using exclusive reactions within the data samples to match the widths of the ΔP distributions in both the experimental data and Monte Carlo files. These methods have not been fully updated and checked for the lower beam energies but will be incorporated into the final analysis.

D. Data vs MC Comparison

The clasdis MC has repeatedly been shown to be an effective tool for describing CLAS12 SIDIS data. As we use the Monte Carlo for the majority of our studies in this proposal (limited by the lack of any RG-K inbending data) we provide several examples of comparisons between clasdis MC and existing CLAS12 data. In Fig. 4 the reconstructed clasdis MC is compared to collected CLAS12 RG-K data for 6.5 and 7.5 GeV. Excellent agreement is observed for the integrated samples. As further examples,

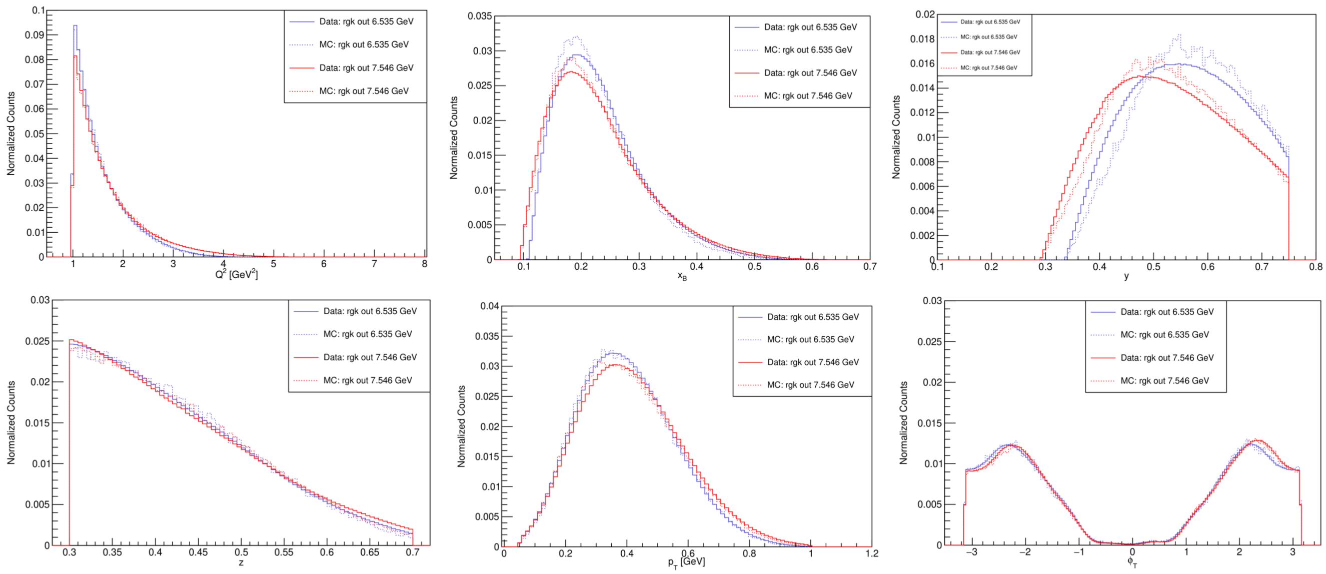

FIG. 4: Comparisons between the clasdis MC (dotted lines) and collected CLAS12 data (solid lines) for 6.5 GeV (blue) and 7.5 GeV (red). The top row shows relevant DIS variables (Q^2, x_b and y) and the bottom row shows relevant SIDIS variables (z, P_T and ϕ. The datasets have been normalized to the total number of π^+ in order to allow a direct comparison of the shapes of the distributions.

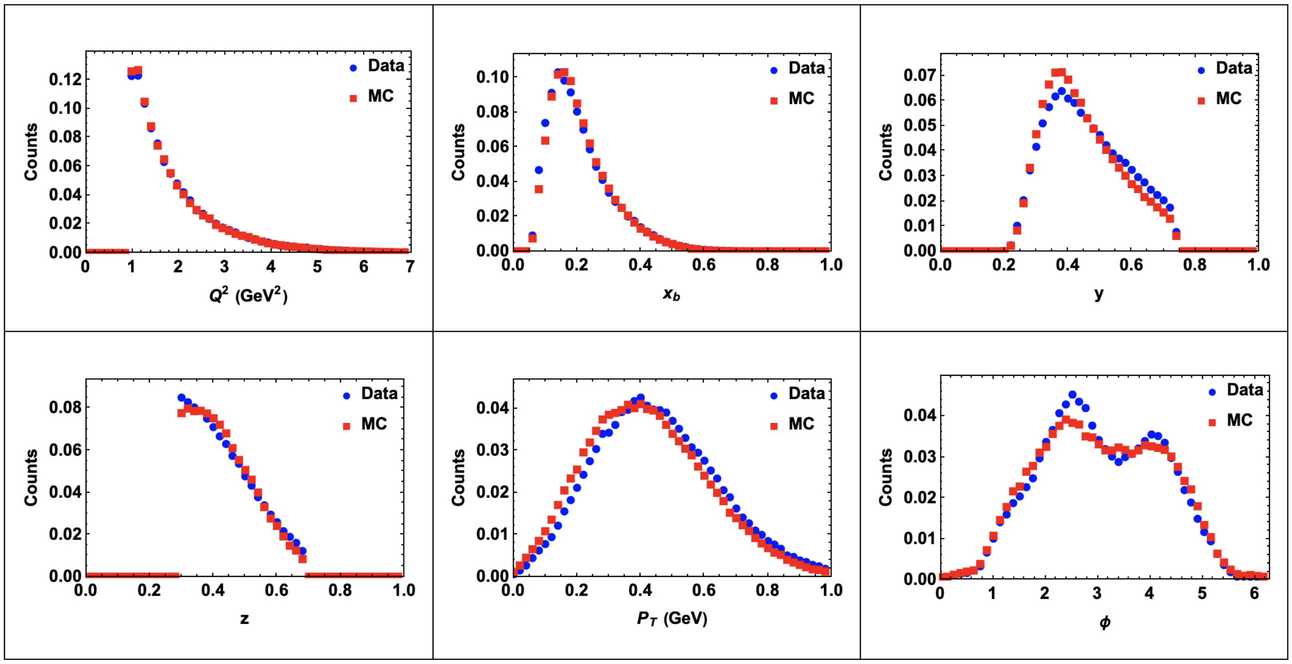

FIG. 5: Comparisons between the integrated outbending 10.6 GeV clasdis MC (red) and RGA Fall18 outbending 10.6 GeV data (blue) samples for Q^2, x_b, y, z, P_T and ϕ without resolution smearing. Good agreement is observed in general. Some slight differences are observed for the y and P_T distributions (the difference in ϕ can be explained by the lack of unpolarized modulations in the clasdis generator). The datasets have been normalized to the total number of π^+ in order to allow a direct comparison of the shapes of the distributions.

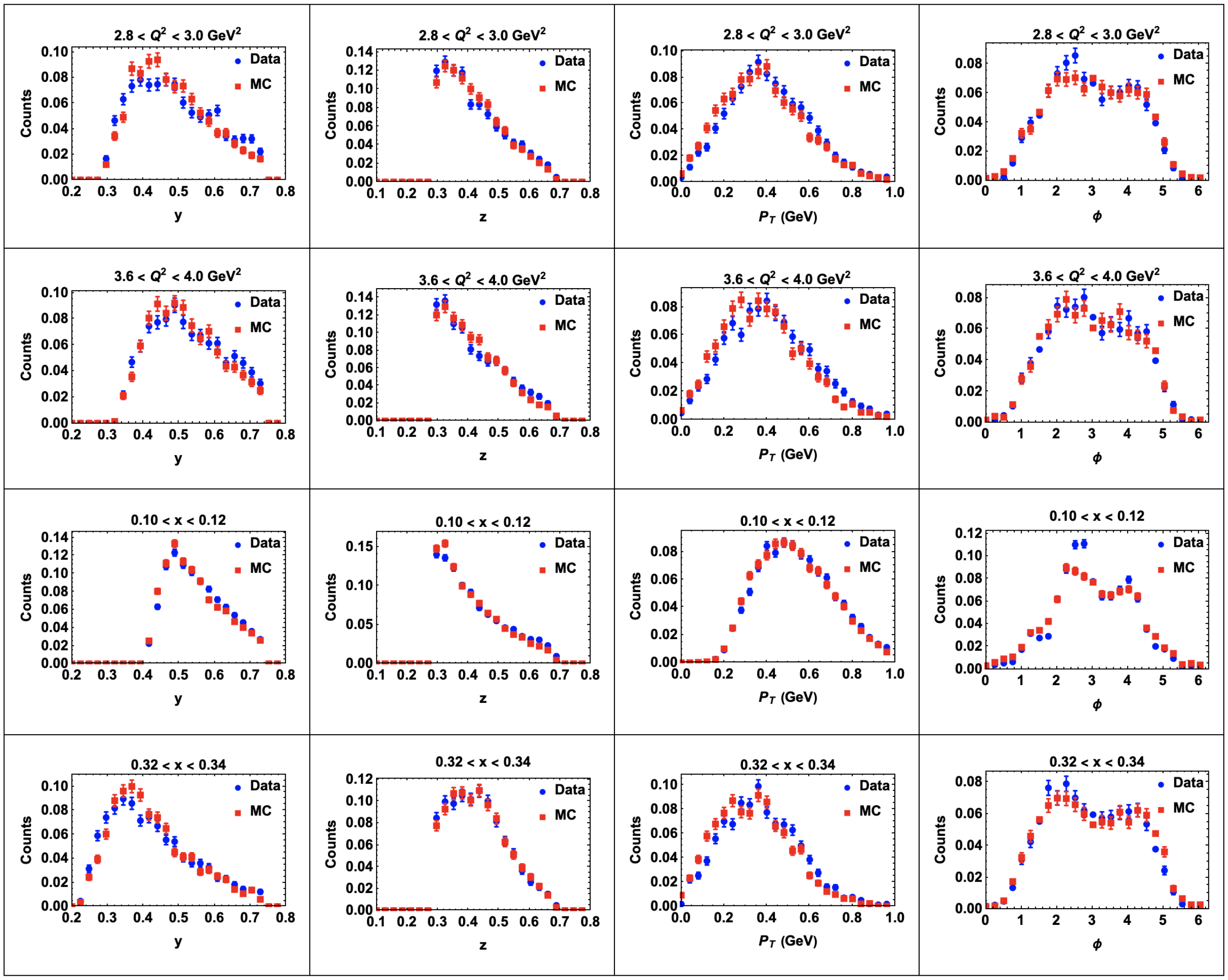

FIG. 6: Comparisons between the integrated outbending 10.6 GeV clasdis MC (red) and RGA Fall18 outbending 10.6 GeV data (blue) samples for y, z, P_T and ϕ without resolution smearing in various bins of Q^2 and x_b (note that the specific bin $0.32 < x_b < 0.34$ and $2.8 < Q^2 < 3.0$ is used for statistic projections in the following sections). The datasets have been normalized to the total number of π^+ in order to allow a direct comparison of the shapes of the distributions.

IV. ANALYSIS PROCEDURE

A. Particle Identification and Fiducial Cuts

The particle identification procedure for SIDIS events has been studied extensively in CLAS12 analyses. Similarly, the geometric fiducial cuts necessary to remove detector edge cases, where particle momenta may not be reconstructed accurately, have been thoroughly investigated. We will follow the general outline of previous experiments, allowing for the possibility of slight refinements and adjustments with the forthcoming "pass-2" software and future data requirements.

B. Channel Selection

For each event, we identify an electron and pion candidate using the particle identification scheme developed for the CLAS12 EventBuilder [36] along with the additional cuts that have been discussed above. The selection of electron and hadron candidates allows for the calculation of various kinematics on an event-by-event basis. The final SIDIS events will be selected with the following list of preliminary cuts:

- $Q^2 > 1.00$ GeV^2, to select DIS events.
- $W > 2.00$ GeV, in order to avoid the resonance region.
- $y < 0.75$, in order to avoid the region most susceptible to radiative effects.
- $M_x > 1.50$ GeV, in order to avoid contributions from exclusive production, e.g. $ep \to e'N\pi^+$, $ep \to e'\Delta^0\pi^+$, etc.
- $x_F > 0$, in order to limit contributions from target fragmentation.
- $0.3 \leq z \leq 0.7$ in order to avoid target fragmentation and exclusive channels while focusing on the SIDIS region.

C. Rosenbluth Separation

Using simulations for the three different beam energies, 6.5 GeV, 7.5 GeV, and 10.6 GeV, cross sections are estimated for different x_B-Q^2 bins. For a particular x_B-Q^2 bin, and for integrated z, P_T and ϕ, the cross sections can be expressed by a constant term G, $K(y)$, and ϵ as

$$\frac{d\sigma}{dxdQ^2dzdP_T} = GK(y)\left(F_{UU,T} + \epsilon F_{UU,L}\right). \tag{11}$$

We use the Rosenbluth L/T separation procedure to further separate $F_{UU,T}$ and $F_{UU,L}$. To perform Rosenbluth procedure, it is necessary to vary ϵ by keeping Q^2 and x_B fixed, which can only be done by varying the beam energy. In this proposal, we will use three beam energies 6.535, 7.546, and 8.4 GeV from the inbending RG-K run and 10.6 GeV from the inbending RG-A run. The procedure to extract $F_{UU,T}$ and $F_{UU,L}$ is then to apply a straight line to extracted $F_{UU,T} + \epsilon F_{UU,L}$ values for different ϵ points at each fixed Q^2 and x_B point. The intercept at $\epsilon = 0$ yields $F_{UU,T}$ and the slope gives $F_{UU,L}$.

The procedure for L/T separation was first tested with MC data sets for 6.535, 7.546, 8.4 and 10.6 GeV beam energies. MC banks include the information on the integrated over the whole covered kinematics cross sections, allowing to define integrated cross sections in any given bin. With resolutions in kinematic variables the choice of 0.02 step in x_B and 0.2 in Q^2 was tested (still factor of 4-5 better than resolutions of CLAS12 expected from MC). Distributions over electron angles and energies in the CLAS12 for a given bin ($0.3 < x < 0.32$, $2.8 < Q^2 < 3.0$, $0.2 < z < 0.7$, and $0.2 < P_T < 0.6$) are shown in Fig. 7. The corresponding integrated cross sections for that bin calculated from MC initial integrated cross sections is shown in Fig. 12. The distributions of $e'\pi^+X$ events over the variables y and ϵ are shown in Fig. 8. They were used to calculate the kinematic factors and extract the part of the cross section that depends on the SFs.

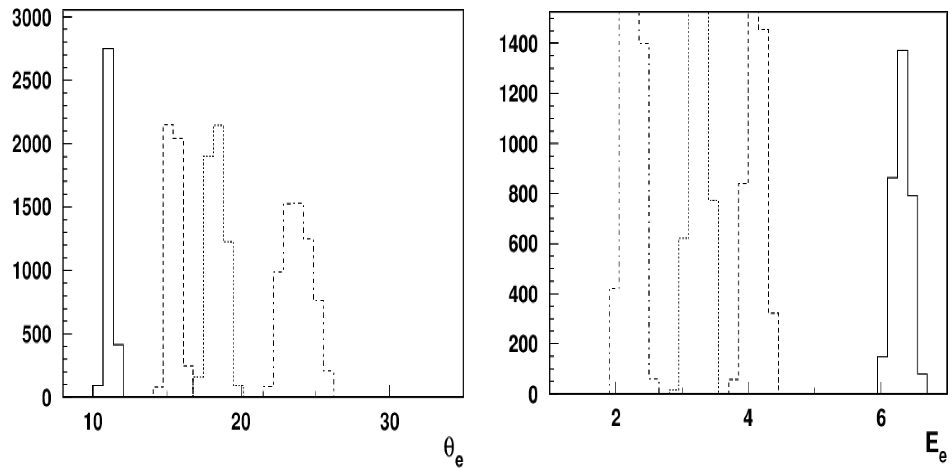

FIG. 7: Distributions of scattered electrons angles (left) and momenta (right) for 4 beam energies for a bin ($0.3 < x < 0.32$, $2.4 < Q^2 < 2.6$, $0.2 < z < 0.7$, and $0.2 < P_T < 0.6$). The solid line is for the beam energy 10.6 GeV, dashed for 7.5 GeV, dotted 7.5 GeV and dash-dotted for 6.535 GeV

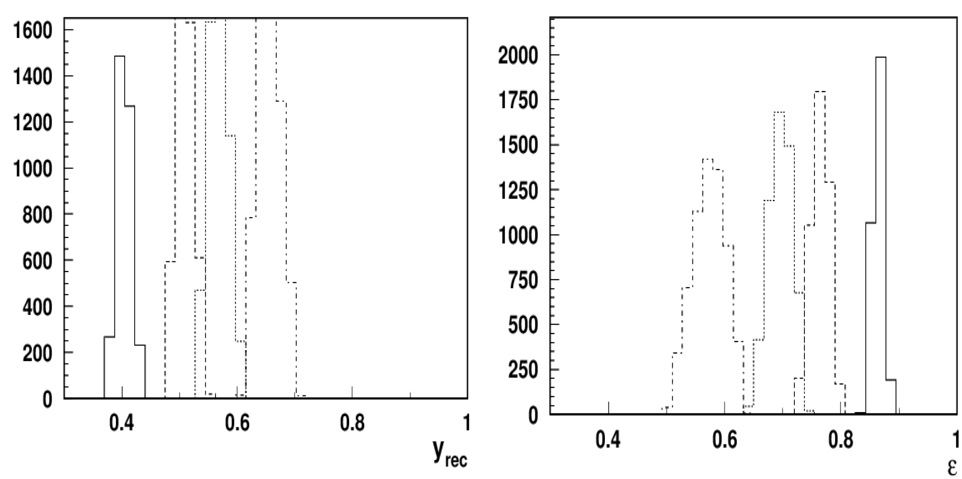

FIG. 8: Distributions of scattered electrons for $y = \nu/E$ (left) and ϵ (right) for 4 beam energies for a bin ($0.3 < x < 0.32$, $2.4 < Q^2 < 2.6$, $0.2 < z < 0.7$, and $0.2 < P_T < 0.6$).

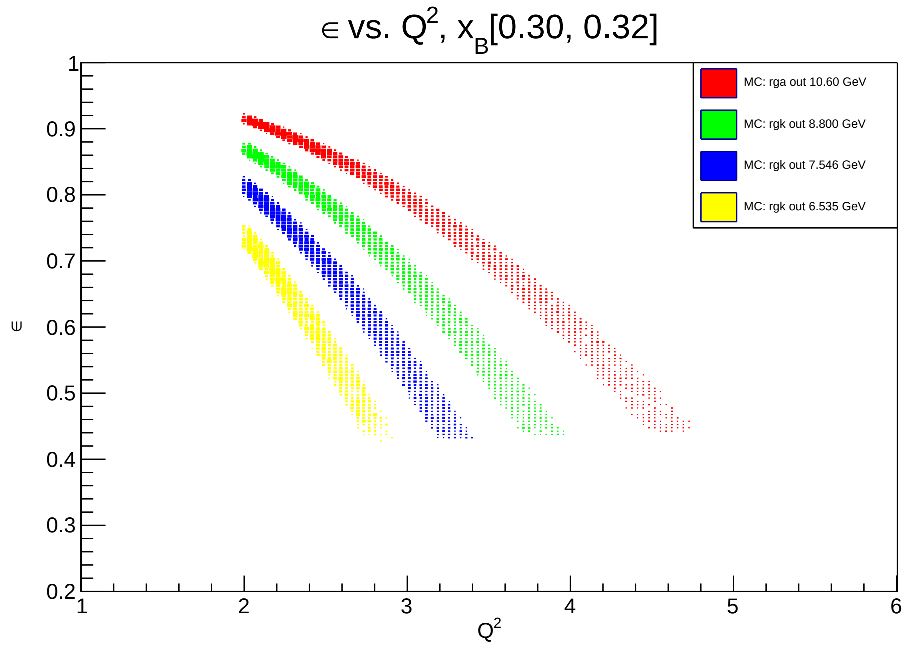

FIG. 9: The ϵ-term as a function of Q^2 for all four beam energies in the outbending torus polarity configuration for the given x_B bin.

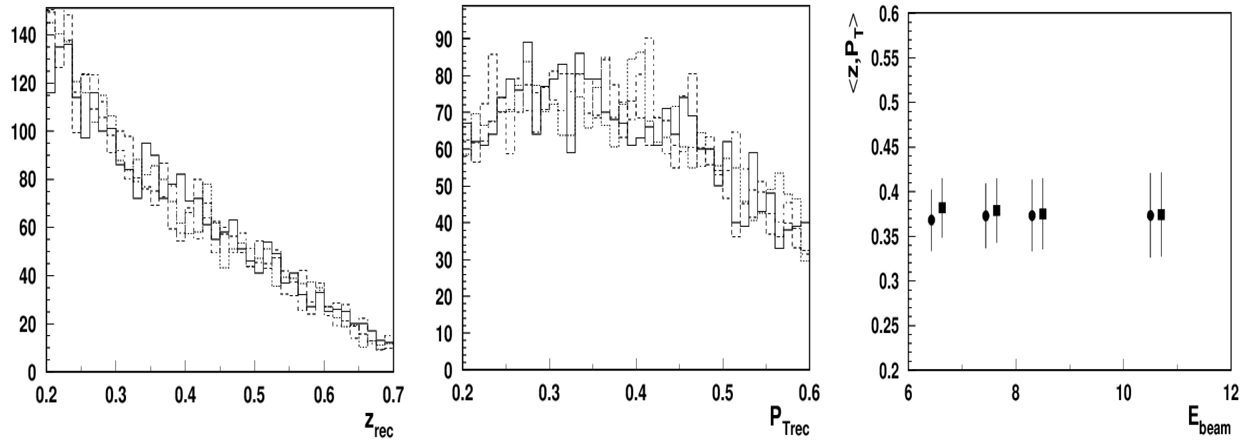

FIG. 10: z (left) and P_T (middle), normalized to same number of events, distributions of $ep \to e'\pi^+X$ events in a given bin from Figs. 7,8. The right panel shows the averages of z (circles) and P_T (squares) vs beam energy.

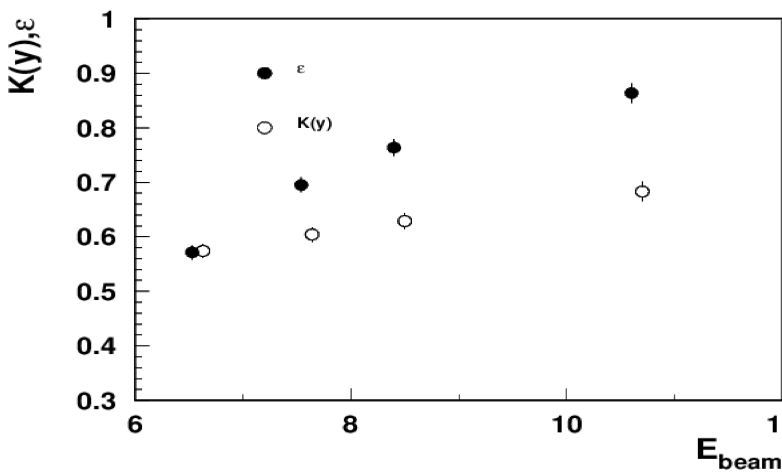

FIG. 11: Dependencies of the ϵ and $K(y)$ on the beam energy in a given bin from Figs. 7,8.

The distributions over the π^+ variables z and P_T for all beam energies, shown in Fig. 10, are similar, and were checked to have averages the same within 1-2%.

The average values of ϵ and the kinematic factor $K(y)$, shown in Fig. 11

The dependence of the cross section scaled with the value of the kinematic factor $K(y)$ (Fig.12) is expected to have the beam energy dependence localized only in the term $\epsilon F_{UU,L}$ and can be used to extract the ratio R. R is not supposed to depend on the beam energy, neither $F_{UU,T}$ and $F_{UU,L}$, and that can be checked using different energy settings. The value of R extracted from the clasdis MC simulation for the bin shown in Fig. 12 using a combination of 4 beam energies is shown in Fig. 13. A similar procedure will be applied to the combined RGK (6.5,7.5) and RGA (10.6) data.

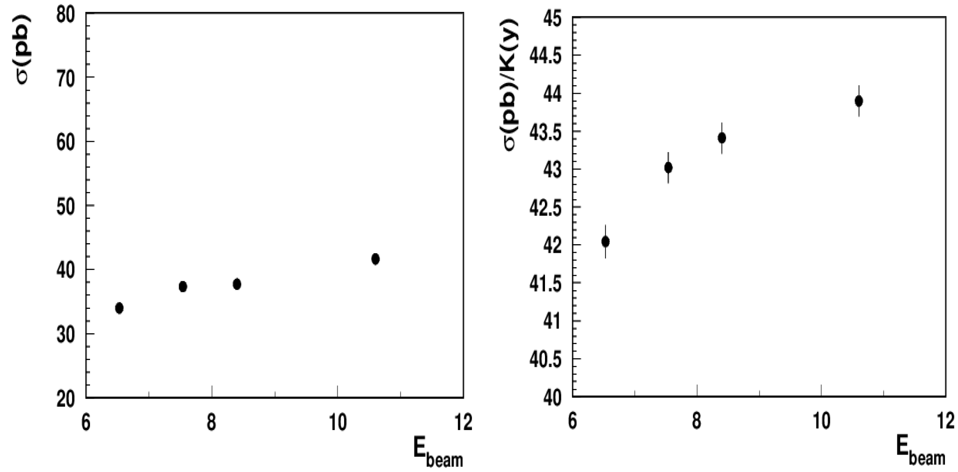

FIG. 12: The integrated cross section in a given bin as a function of the beam energy (left) and the same cross section scaled by the energy-dependent kinematic factor (right) for a single bin (see Figs7-11).

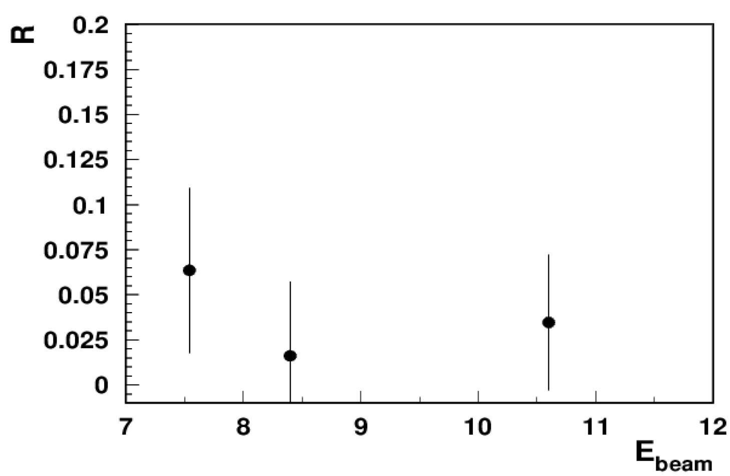

FIG. 13: The value of R plotted for different beam energies for a single bin (see Figs7-12) .

Systematic uncertainties have been studied in detail for previous RG-A SIDIS analyses.

D. Minor Systematic Uncertainties

Different sources of systematic uncertainty have been evaluated and were found to be small. First the effect of PID related contamination of the SIDIS sample were found to be well under control. With a cut on p $<$ 5 GeV (or corresponding z cuts to account for the separate beam energies) and additional cuts on the χ^2 value from the PID system, the kaon contamination in the pion sample is in the order of 1 - 2% for most kinematic bins. After a cut on $M_X > 1.5$ GeV, also the contamination from baryon resonances is well under control and at the level of a few percent for most kinematic bins. With a cut on y $<$ 0.75 also the contamination from charge symmetric background was found to be less than 1% for most kinematic bins.

E. Acceptance Correction

Different acceptance correction methods have been compared. It was found that the results from the different methods agree well and after a further tuning of the simulations, an uncertainty of a few percent can be assumed for this source. However, compared to the other uncertainties this source is expected to be one of the major contributions to the systematic uncertainty.

F. Radiative Effects

Radiative photons emitted in the scattering process modify the reconstructed virtual photon's 4-momentum. This introduces a bias in the SIDIS event kinematics that needs to be corrected for. These radiative corrections on the measured amplitudes are expected to be small for our measurements because of the requirement to detect hadrons in the final state. This limits the radiative corrections to those for the inelastic part of the cross section, unlike for inclusive deep inelastic scattering. In addition to the requirement to produce multiple final-state hadrons, a cut on the energy of the virtual photon relative to the incoming electron ($y < 0.75$) was imposed. Various methods involving the evaluation of Monte Carlo simulations using the dedicated software (RADGEN) in combination with LEPTO have been used in previous CLAS12 SIDIS measurements. In general the estimated contributions to the systematic uncertainty remain small, on the order of a few percent per bin.

G. Total systematic uncertainty

In agreement with previous studies the total systematic uncertainty is expected to be on the order of 10%.

V. CONCLUSIONS

Our proposed addition to the Run Group K experiments aims to provide an in-depth analysis of semi-inclusive deep inelastic scattering (SIDIS) cross sections for π^+ production. By comparing our results with those from Run Group A and performing a Rosenbluth separation from measurements at different ratios of the longitudinal and tangential photon flux we will be able to disentangle the separate contributions to the SIDIS cross section.

There is a significant gap in our current understanding of the nucleon structure and quark-gluon dynamics, as there have been no direct measurements of R_{SIDIS} for the semi-inclusive deep inelastic scattering process. Previous measurements have relied on the assumption that $R_{\text{SIDIS}} = R_{DIS}$, which introduces considerable uncertainties when using SIDIS data to deduce quark flavor and spin distributions. Our study is designed to fill this knowledge gap by providing valuable insights into the nucleon structure and quark-gluon dynamics through direct measurements of R_{SIDIS}.

This research will not only contribute to a more accurate and comprehensive understanding of the nucleon structure, but will also help to refine existing theoretical models and calculations. The direct measurement of R_{SIDIS} will allow for more precise determinations of quark distributions and their interactions within the nucleon, ultimately enhancing our knowledge of the fundamental building blocks of matter.

[1] M. Anselmino, A. Mukherjee, and A. Vossen, "Transverse spin effects in hard semi-inclusive collisions," *Prog. Part. Nucl. Phys.*, vol. 114, p. 103806, 2020.

[2] A. Bacchetta, M. Diehl, K. Goeke, A. Metz, P. J. Mulders, and M. Schlegel, "Semi-inclusive deep inelastic scattering at small transverse momentum," *JHEP*, vol. 02, p. 093, 2007.

[3] J. Gao, L. Harland-Lang, and J. Rojo, "The Structure of the Proton in the LHC Precision Era," *Phys. Rept.*, vol. 742, pp. 1–121, 2018.

[4] J. J. Ethier and E. R. Nocera, "Parton Distributions in Nucleons and Nuclei," *Ann. Rev. Nucl. Part. Sci.*, vol. 70, pp. 43–76, 2020.

[5] A. Metz and A. Vossen, "Parton Fragmentation Functions," *Prog. Part. Nucl. Phys.*, vol. 91, pp. 136–202, 2016.

[6] A. Kotzinian, “New quark distributions and semiinclusive electroproduction on the polarized nucleons,” *Nucl. Phys.*, vol. B441, pp. 234–248, 1995.

[7] P. J. Mulders and R. D. Tangerman, “The complete tree-level result up to order 1/q for polarized deep-inelastic leptoproduction,” *Nucl. Phys.*, vol. B461, pp. 197–237, 1996.

[8] S.-y. Wei, Y.-k. Song, K.-b. Chen, and Z.-t. Liang, “Twist-4 contributions to semi-inclusive deeply inelastic scatterings with polarized beam and target,” *Phys. Rev. D*, vol. 95, no. 7, p. 074017, 2017.

[9] C. J. Bebek, A. Browman, C. N. Brown, K. M. Hanson, R. V. Kline, D. Larson, F. M. Pipkin, S. W. Raither, A. Silverman, and L. K. Sisterson, “Charged Pion Electroproduction from Protons Up to Q**2 = 9.5-GeV**2,” *Phys. Rev. Lett.*, vol. 37, pp. 1525–1528, 1976.

[10] A. Bacchetta, D. Boer, M. Diehl, and P. J. Mulders, “Matches and mismatches in the descriptions of semi-inclusive processes at low and high transverse momentum,” *JHEP*, vol. 08, p. 023, 2008.

[11] F. D. Aaron *et al.*, “Measurement of the Inclusive e\pmp Scattering Cross Section at High Inelasticity y and of the Structure Function F_L,” *Eur. Phys. J. C*, vol. 71, p. 1579, 2011.

[12] Y. Liang *et al.*, “Measurement of R=σL/σT and the separated longitudinal and transverse structure functions in the nucleon-resonance region,” *Phys. Rev. C*, vol. 105, no. 6, p. 065205, 2022.

[13] V. D. Burkert *et al.*, “The CLAS12 Spectrometer at Jefferson Laboratory,” *Nucl. Instrum. Meth. A*, vol. 959, p. 163419, 2020.

[14] S. Kuhn *et al.*, “Jlab experiment e12-06-109,” 2006.

[15] H. Avakian *et al.*, “Studies of spin-orbit correlations in pion electroproduction in dis with polarized hydrogen and deuterium targets,” *JLab Experiment E12-07-107*, 2007.

[16] K. Hafidi *et al.*, “Jlab experiment e12-09-007b,” 2009.

[17] H. Avakian *et al.*, “Studies of spin-orbit correlations in kaon electroproduction in dis with polarized hydrogen and deuterium targets,” *JLab Experiment E12-09-009*, 2009.

[18] S. Niccolai *et al.*, “Jlab experiment e12-06-109a,” 2006.

[19] C. Dilks *et al.*, “Studies of dihadron electroproduction in dis with longitudinally polarized hydrogen and deuterium targets,” *JLab Experiment E12-09-007A*, 2019.

[20] Y. Sharabian *et al.*, “The CLAS12 high threshold Cherenkov counter,” *Nucl. Instrum. Meth. A*, vol. 968, p. 163824, 2020.

[21] M. Ungaro *et al.*, “The CLAS12 Low Threshold Cherenkov detector,” *Nucl. Instrum. Meth. A*, vol. 957, p. 163420, 2020.

[22] M. Contalbrigo *et al.*, “The CLAS12 Ring Imaging Cherenkov detector,” *Nucl. Instrum. Meth. A*,

vol. 964, p. 163791, 2020.

[23] M. D. Mestayer *et al.*, “The CLAS12 drift chamber system,” *Nucl. Instrum. Meth. A*, vol. 959, p. 163518, 2020.

[24] D. Carman *et al.*, “The CLAS12 Forward Time-of-Flight system,” *Nucl. Instrum. Meth. A*, vol. 960, p. 163629, 2020.

[25] G. Asryan *et al.*, “The CLAS12 forward electromagnetic calorimeter,” *Nucl. Instrum. Meth. A*, vol. 959, p. 163425, 2020.

[26] M. Antonioli *et al.*, “The CLAS12 Silicon Vertex Tracker,” *Nucl. Instrum. Meth. A*, vol. 962, p. 163701, 2020.

[27] D. Carman *et al.*, “The CLAS12 Central Time-of-Flight system,” *Nucl. Instrum. Meth. A*, vol. 960, p. 163626, 2020.

[28] A. Acker *et al.*, “The CLAS12 Micromegas Vertex Tracker,” *Nucl. Instrum. Meth. A*, vol. 957, p. 163423, 2020.

[29] M. Ungaro *et al.*, “The CLAS12 Geant4 simulation,” *Nucl. Instrum. Meth. A*, vol. 959, p. 163422, 2020.

[30] H. Avakian, “clasdis.” `https://github.com/JeffersonLab/clasdis`, 2020.

[31] T. Sjostrand, S. Mrenna, and P. Z. Skands, “PYTHIA 6.4 Physics and Manual,” *JHEP*, vol. 0605, p. 026, 2006.

[32] L. Mankiewicz, A. Schafer, and M. Veltri, “PEPSI: A Monte Carlo generator for polarized leptoproduction,” *Comput. Phys. Commun.*, vol. 71, pp. 305–318, 1992.

[33] G. Ingelman, A. Edin, and J. Rathsman, “LEPTO 6.5: A Monte Carlo generator for deep inelastic lepton - nucleon scattering,” *Comput.Phys.Commun.*, vol. 101, pp. 108–134, 1997.

[34] T. B. Hayward, “Dihadron beam spin asymmetries on an unpolarized hydrogen target with CLAS12.” Thesis, College of William & Mary, available at `https://www.jlab.org/Hall-B/general/thesis/THayward_thesis.pdf`, 2021.

[35] CLAS, “11 GeV polarized electrons on liquid hydrogen target to study proton structure, 3d imaging, and gluonic excitations, RG-A analysis overview and procedure.” Internal Note, under review. Snapshot from August 2020: `https://clas12-docdb.jlab.org/DocDB/0009/000949/001/RGA_Analysis_Overview_and_Procedures-08172020.pdf`.

[36] V. Ziegler *et al.*, “The CLAS12 software framework and event reconstruction,” *Nucl. Instrum. Meth. A*, vol. 959, p. 163472, 2020.